

## Resonant photoemission spectra at the $4f$ and $5p$ levels of Tm across the $4d$ - $4f$ absorption threshold

C. L. Nicklin, C. Binns, S. Mozley, and C. Norris

*Department of Physics and Astronomy, University of Leicester, Leicester LE1 7RH, United Kingdom*

E. Alleno and M-G. Barthés-Labrousse

*Centre d'Etudes de Chimie Metallurgique, CNRS, Vitry Cedex, France*

G. van der Laan

*Council for the Central Laboratory of the Research Councils, Daresbury Laboratory, Warrington WA4 4AD, United Kingdom*

(Received 12 December 1994; revised manuscript received 1 May 1995)

The decay of the  $4d$  core hole in the rare-earth metal thulium, following resonant absorption into the  $4f$  level, has been monitored by photoelectron spectroscopy and compared with calculations predicting the  $4f$  and  $5p$  electron distribution curves. The Tm, deposited on a cooled Ag surface to stabilize both trivalent and divalent states, shows three strong peaks in the total electron yield spectrum. The first absorption peak ( ${}^3H_6$ ) results in a resonant enhancement of predominantly the  $5s$  and  $5p$  emission, together with an increase in the trivalent  $4f$  emission. The weaker absorption peak ( ${}^3H_5$ ) leads to a relatively small increase in the emission through the trivalent  $4f$  state. The last absorption peak ( ${}^3G_5$ ) shows a strong enhancement of two specific channels, at higher binding energy, within the trivalent  $4f$  emission. The divalent  $4f$  emission is only enhanced near the  ${}^3H_6$  resonance.

### I. INTRODUCTION

Rare-earth (RE) metals are characterized by an outer electronic structure comprised of incompletely filled and localized  $4f$  states which overlap the extended  $5d6s$  valence orbitals. This is responsible for a variety of unique effects, such as valence fluctuations<sup>1</sup> and heavy fermion behavior.<sup>2</sup> Another process which can occur as a consequence of the localization of the  $4f$  states is resonant absorption,<sup>3-19</sup> when a core electron, from for example the  $4d$  shell, is excited into an empty  $4f$  orbital,  $4d^{10}4f^n \rightarrow 4d^9 4f^{n+1}$ . Absorption occurs close to the core ionization threshold due to the low binding energy of the  $4f$  level. The resonant absorption can be spread over a broad energy range in excess of 20 eV as a result of the extent of the excited state ( $4d^9 4f^{n+1}$ ) multiplet structure,<sup>7</sup> which is primarily a consequence of the electrostatic interactions between the  $4f$  electrons and the  $4d$  core hole. Following absorption, the atom may decay via several routes, such as deexcitation of an electron from a  $5p$  level into the  $4d$  hole with the emission of a  $4f$  electron. Throughout this paper, this type of process is referred to as a  $4d5p4f$  decay. Such decay routes may produce electrons with the same energy as directly emitted photoelectrons (from the  $5p$  shell in the example above), although some transitions can result in the appearance of additional peaks at different energies.<sup>20,21</sup> The study of the hole decay following absorption allows details of intra-atomic processes to be monitored.

Recent experimental studies of resonant photoemission in RE's have focused on  $4d$ - $4f$  absorption and subsequent decay routes in La, Gd, and Eu<sup>22,23</sup> which are at the low mass end (La) and in the middle (Gd, Eu) of the RE series.

In La a narrow absorption peak occurs at a lower energy than an intense and broad giant resonance.<sup>6</sup> Decay is found to be predominantly via resonant Auger processes (the originally promoted electron is not involved in the decay) for the narrow peak and autoionization leading to  $5p^{-1}$  or  $5s^{-1}$  states for the giant resonance (the number after the negative sign indicates the number of holes left in the energy level). The results for Gd and Eu again show narrow absorption peaks prior to the large giant resonance. The excitations were found to decay mainly by autoionization, in the narrow peaks to  $5p^{-1}$  or  $5s^{-1}$  final states and for the giant resonance to a  $4f^{-1}$  one-hole state. Resonant Auger processes for the narrow absorption and normal Auger processes for the giant resonance were also found to be significant decay channels.

As a free atom, thulium (Tm) is divalent but in the solid, the trivalent  $4f^{12}$  configuration is favored, leaving two unoccupied  $4f$  orbitals into which electrons can be excited. Thulium is therefore a relatively simple system to study as the number of possible decay channels is reduced in comparison to most of the RE series. Resonant absorption in Tm systems has been reported earlier, but a detailed analysis of the spectra has not been performed. Johansson, Allen, and Lindau<sup>24</sup> made limited photoemission measurements of Tm metal, in the energy range 100–200 eV, but no explanation as to the origin of resonant effects was given. Oh, Allen, and Lindau<sup>25</sup> have studied resonant photoemission in mixed valence TmSe and found resonant enhancement of both states at energies close to the Tm  $4d$  binding energy. Again, however, there is no indication of the decay processes following absorption. Other theoretical and experimental studies of the absorption process have been reported,<sup>3-19</sup> but none

of these have calculated the enhanced photoemission features which may be produced by the hole decay. Off-resonant photoemission features of trivalent and divalent Tm have previously been calculated by considering the fractional parentage coefficients derived from the theoretical transitions  $4f^{12} \rightarrow 4f^{11}$  and  $4f^{13} \rightarrow 4f^{12}$ , respectively.<sup>26</sup>

We present measurements of the  $5s$ ,  $5p$ , and  $4f$  photoelectron spectra of Tm as a function of photon energy through the  $4d$ - $4f$  absorption threshold. The spectra are compared with the results of calculations using a model in which the decay processes are described by the atomic Hartree-Fock plus statistical exchange approximation. In Sec. III, details of the calculational method are explained; the results are presented and discussed in Sec. IV.

## II. EXPERIMENT

Total electron yield and photoemission spectra were recorded at the Daresbury Synchrotron Radiation Source (SRS) on beamline 6.1, using photons in the energy range 100–200 eV.

Experiments were performed, in an ultrahigh-vacuum (UHV) chamber with a base pressure of  $5 \times 10^{-11}$  mbar, on thick ( $> 100$  Å) Tm layers grown on an Ag(001) surface. The sample was cooled to 150 K prior to deposition, in order to observe the absorption and resonant behavior of divalent Tm, in addition to the trivalent Tm.<sup>27</sup> An additional sample was prepared for each measurement, by evaporating Tm from a tantalum-lined crucible in a Knudsen cell surrounded by a water-cooled shroud. Contamination (carbon, oxygen, sulfur) levels were monitored by Auger electron spectroscopy (AES), and were never observed to be greater than 2% of the Tm 169-eV Auger peak.

Total yield spectra were recorded by measuring the sample drain current as a function of photon energy in the range 150–200 eV. The electron energy distribution curves (EDC's) were recorded with a VSW HA-100 hemispherical analyzer using multichannel detection, in fixed analyzer transmission mode (FAT 4.4). All measurements were made with the analyzer in the same horizontal plane as the incoming beam, and the sample positioned such that the angle of incidence and the outgoing angle to the analyzer were both  $45^\circ$  with respect to the sample normal. The EDC's were normalized to account for the variation in monochromator transmission at different photon energies. The total resolution was 200 meV at a photon energy of 135 eV, as measured at the Fermi edge.

## III. CALCULATIONAL DETAILS

The ground-state configuration of bulk Tm is  $4f^{12}5s^25p^65d^16s^2$ . Since the interaction of the  $4f$  electrons with the  $5d$  electron is small and the other shells are completely filled, only the  $4f^{12}$  configuration is considered. The initial state is split by the  $4f$ - $4f$  Coulomb interaction with Slater integrals  $F^2$ ,  $F^4$ , and  $F^6$  resulting in a Hund's rule ground state  $^3H_6$ , which is mixed with

$0.08\%$   $^1I_6$  due to the  $4f$  spin-orbit interaction. The excited state, after  $N_{3,4}$  absorption, has a  $\underline{4d}4f^{13}$  configuration, where a  $4d$  core electron has been excited into the localized  $4f$  shell; the underscore indicates a hole in the shell. This configuration shows a multiplet structure due to splitting by the  $4d$  and  $4f$  spin-orbit interaction and the  $4f$ - $4f$  and  $4d$ - $4f$  Coulomb and exchange interactions. Dipole transitions from the ground state are allowed to the  $^3H_6$ ,  $^3H_5$ ,  $^3G_5$ , and  $^1H_5$  levels. The transition to the  $^1H_5$  state at 12 eV above the  $^3G_5$  is spin forbidden, but obtains a very small intensity due to the spin-orbit interaction.

The divalent Tm  $4f^{13}$  configuration has a ground state of  $^2F_{7/2}$ , and x-ray absorption is allowed to the  $^2D_{5/2}$  level of the configuration  $\underline{4d}4f^{14}$ . The excited state  $\underline{4d}4f^{n+1}$  can decay to the final states of  $4f^{n-1}\epsilon$ ,  $\underline{5p}4f^n\epsilon$ ,  $\underline{5s}4f^n\epsilon$ ,  $\underline{5p}^24f^{n+1}\epsilon$ ,  $\underline{5s}5p4f^{n+1}\epsilon$ , or  $\underline{5s}^24f^{n+1}\epsilon$ , where  $\epsilon$  is a continuum level. In these configurations, only the first three can be accessed by direct photoemission, namely  $4f \rightarrow \epsilon$ ,  $5p \rightarrow \epsilon$ , and  $5s \rightarrow \epsilon$ , respectively. These states therefore show interference with the decay process.

The parameters for the ionic rare-earth configurations in spherical symmetry were calculated using Cowan's code.<sup>28</sup> This uses the Hartree-Fock plus statistical exchange (HX) method to evaluate the Slater integrals, spin-orbit constants, and matrix elements for the dipole and Auger transitions (see Tables I and II). To include intra-atomic correlation effects, the  $F^k(f,f)$  integrals were reduced to 80%, the  $F$  and  $G^k(c,f)$  integrals to 60%, and the Auger matrix elements  $R$  to 75% for the calculation of the absorption and resonant photoemission spectra.

These spectra were calculated from the  $4f^n$  ground state by taking into account radiative transitions to first order to the  $4f^{n-1}\epsilon$  configuration, and Auger transitions to infinite order to the  $4f^{n-1}\epsilon$  and  $\underline{5p}4f^n\epsilon$  configurations.<sup>16</sup> The direct photoemission has dipole matrix elements  $\langle l||r||k \rangle$  with  $k = l \pm 1$ . The  $l_1 l_2 l_3$  decay has Auger matrix elements  $\langle R(l_1, l_2; l_3, k) \rangle$  with  $k = 0, 2, \dots, k_n$  for  $k_n$  even, and  $k = 1, 3, \dots, k_n$  for  $k_n$  odd, where  $k_n = l_1 + l_2 + l_3$ . Thus for the  $4d4f4f$  process

TABLE I. Hartree-Fock values (eV) of the Slater and spin-orbit parameters for the initial, excited, and final state in the Tm  $4d$  resonant photoemission, obtained by Cowan's code (Ref. 28).

Configuration	$4f^{12}$	$4d^9 4f^{13}$	$5p^5 4f^{12}$	$4f^{13}$	$4d^9 4f^{14}$	$5p^5 4f^{13}$
$F^2(f,f)$	16.469		16.710			
$F^4(f,f)$	10.330		10.494			
$F^6(f,f)$	7.431		7.552			
$\zeta(4f)$	0.333	0.338	0.337	0.314		0.318
$\zeta(4d)$		3.293	4.149		3.271	3.779
$F^2(4d,c)$		18.464	7.115			6.865
$F^4(4d,c)$		11.800				
$G^1(4d,c)$		21.672				
$G^2(4d,c)$			3.474			3.542
$G^3(4d,c)$		13.653				
$G^4(4d,c)$			2.720			2.717
$G^5(4d,c)$		9.666				

TABLE II. Hartree-Fock values of the dipole, and Coster-Kronig matrix elements for the Tm 4*d* resonant photoemission, obtained by Cowan's code (Ref. 28).

Transition	Reduced matrix elements
$f^{12}$	
4 <i>d</i> → 4 <i>f</i>	$\langle 4d    r    4f \rangle = 0.99601$ a.u.
4 <i>d</i> 4 <i>f</i> 4 <i>f</i> decay	$\langle 4f    r    \epsilon_d \rangle = 0.03237$ a.u./ $\sqrt{\text{Ry}}$ $\langle 4f    r    \epsilon_g \rangle = -0.27743$ a.u./ $\sqrt{\text{Ry}}$ $R(4d, 4f; 4f, \epsilon_s) = -0.2578$ eV/ $\sqrt{\text{Ry}}$ $R^k(4d, 4f; 4f, \epsilon_d) = 0.0342, 0.0781, 0.0825$ eV/ $\sqrt{\text{Ry}}$ $R^k(4d, 4f; 4f, \epsilon_g) = -3.2922, -1.8625, -1.2508$ eV/ $\sqrt{\text{Ry}}$
4 <i>d</i> 5 <i>p</i> 4 <i>f</i> decay	$\langle 5p    r    \epsilon_s \rangle = 0.03388$ a.u./ $\sqrt{\text{Ry}}$ $\langle 5p    r    \epsilon_d \rangle = -0.01968$ a.u./ $\sqrt{\text{Ry}}$ $R_{d,e}(4d, 4f; 5p, \epsilon_s) = 0.3886, 0.2500$ eV/ $\sqrt{\text{Ry}}$ $R_{d,e}^k(4d, 4f; 5p, \epsilon_d) = 1.3580, 0.8487, 0.4450, 0.4869$ eV/ $\sqrt{\text{Ry}}$ $R_{d,e}^k(4d, 4f; 5p, \epsilon_g) = 0.9000, 0.5166, 0.4385, 0.4054$ eV/ $\sqrt{\text{Ry}}$
$f^{13}$	
4 <i>d</i> → 4 <i>f</i>	$\langle 4d    r    4f \rangle = 0.99723$ a.u.
4 <i>d</i> 4 <i>f</i> 4 <i>f</i> decay	$\langle 4f    r    \epsilon_d \rangle = 0.03498$ a.u./ $\sqrt{\text{Ry}}$ $\langle 4f    r    \epsilon_g \rangle = -0.29461$ a.u./ $\sqrt{\text{Ry}}$ $R(4d, 4f; 4f, \epsilon_s) = -0.2651$ eV/ $\sqrt{\text{Ry}}$ $R^k(4d, 4f; 4f, \epsilon_d) = 0.0156, 0.0742, 0.0824$ eV/ $\sqrt{\text{Ry}}$ $R^k(4d, 4f; 4f, \epsilon_g) = -3.0793, -1.7012, -1.1305$ eV/ $\sqrt{\text{Ry}}$
4 <i>d</i> 5 <i>p</i> 4 <i>f</i> decay	$\langle 5p    r    \epsilon_s \rangle = 0.03592$ a.u./ $\sqrt{\text{Ry}}$ $\langle 5p    r    \epsilon_d \rangle = -0.01729$ a.u./ $\sqrt{\text{Ry}}$ $R_{d,e}(4d, 4f; 5p, \epsilon_s) = 0.3925, 0.2464$ eV/ $\sqrt{\text{Ry}}$ $R_{d,e}^k(4d, 4f; 5p, \epsilon_d) = 1.3806, 0.8467, 0.4430, 0.4822$ eV/ $\sqrt{\text{Ry}}$ $R_{d,e}^k(4d, 4f; 5p, \epsilon_g) = 0.8916, 0.5051, 0.4539, 0.4087$ eV/ $\sqrt{\text{Ry}}$

we have photoemission decay to the *s*, *d*, *g*, *i*, and *l* continua, and direct photoemission to the *d* and *g* continua. For the 4*d*5*p*4*f* process we have photoemission decay to the *s*, *d*, *g*, and *i* continua, and direct photoemission to the *s* and *d* continua. In the calculation we have neglected the emission to *i* and *l* continua, which is small.

The resonant photoemission decay leads to a broadening of each absorption line which is inversely proportional to the decay rate, and which is given by the square of the Auger matrix elements. The lifetime broadening due to the intrinsic and experimental resolutions were artificially included only in the calculated photoelectron spectra by convoluting the line spectra with a Lorentzian of  $\Gamma = 0.12$  eV and a Gaussian of  $\sigma = 0.085$  eV.<sup>29</sup>

Saturation effects, as mentioned in Ref. 3 for the 3*d* edges of the rare-earth elements, will also be important in this case. For the 4*d* absorption, the calculated total transition probability is 22 times larger than for the 3*d*, while depending on the specific peak the linewidth is on average twice as large. This results in a typical absorption length at the Tm *N*<sub>4,5</sub> edge of 10–20 Å. This will lead to strong saturation effects in the measurements, which have not been included in the calculation.

The reduction factors of the Slater integrals determines mainly the spread of the multiplet structure. The reduction factor of the Auger matrix elements determines mainly the peak widths of the separate absorption lines. It was not possible to control, at the same time, the relative peak positions as well as the relative intensities of each peak. Knowing that the relative energies are more

accurate than the relative intensities and also more straightforward to deduce from the proportionality with the reduction factors, we choose for optimization of the energy positions. The intensities of the peaks have, therefore, not been optimized.

## IV. RESULTS AND DISCUSSION

### A. Experimental and calculated absorption spectra

Figure 1(a) shows the measured total electron yield spectrum from the Tm layer. It is composed of three peaks at photon energies of 174.4, 177.5, and 181.3 eV, which are identified with the transitions to the final states <sup>3</sup>H<sub>6</sub>, <sup>3</sup>H<sub>5</sub>, and <sup>3</sup>G<sub>5</sub>, respectively (Ref. 10). There is a very weak fourth transition to a <sup>1</sup>H<sub>5</sub> state, which although spin forbidden is allowed by the spin-orbit interaction. The peak widths and intensities are determined by the magnitude and transition rates of the absorption and decay processes.

Figure 1(b) shows the result of a calculation for the dipole-allowed transitions. It gives the relative positions of the peaks; the absolute energy of the absorption spectrum, which depends on the cohesive energy of the solid, cannot be calculated within an ionic model. The calculation reproduces the triplet of peaks, with widths and intensities dependent on the decay channels; see Sec. III. The energy separations are in excellent agreement with the measured spectrum. The relative intensity of the <sup>3</sup>G<sub>5</sub>

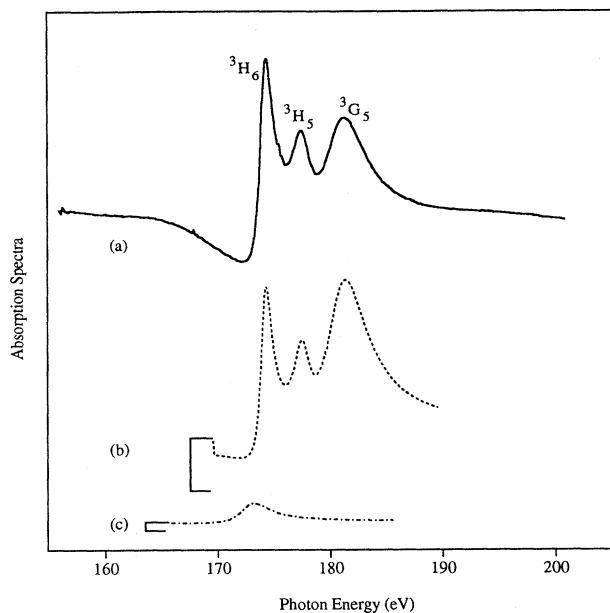


FIG. 1. Total yield spectrum of Tm measured on sample (a) together with calculations of absorption curves for trivalent Tm (b) and divalent Tm (c). Dipole-allowed transitions are labeled in *LS* coupling. The direct photoemission intensity (the non-resonant part) is indicated by the vertical line to the left of each figure.

peak is stronger in the calculated spectrum in comparison to the measured curve. This can be explained as the model allows only for deexcitation of either a  $5p$  or  $4f$  electron into the  $4d$  hole, whereas this process may also occur for the  $5s$  and  $5d$  levels which are neglected in the model.

Divalent Tm has a  $4f^{13}$  configuration, in which only one  $4f$  orbital is vacant. The calculation for divalent Tm is shown in Fig. 1(c) and results in a single absorption peak. The intensity of the absorption has been normalized to the area under the divalent photoemitted peaks (Fig. 2). Although it coincides and is dominated by the trivalent absorption band, the resonant enhancement of the divalent photoemission will be observable since the photoemission features are well separated in energy (Fig. 2).

### B. Electron distribution curves

The decay following absorption is monitored by photoelectron spectroscopy, using photons at the absorption peak energies to excite the emission. Figure 2 shows the full electron distribution curves from 0- to 60-eV binding energy at different photon energies both on and off resonance.

The peaks in the off-resonant spectrum, Fig. 2(a), are assigned as follows. The broad peak centered at a binding energy of 54 eV is due to photoemission from the  $5s$  energy level. The two peaks at 32- and 25-eV binding energy constitute a doublet associated with the trivalent Tm  $5p$  energy levels ( $5p_{1/2}$  and  $5p_{3/2}$ ). The series of peaks

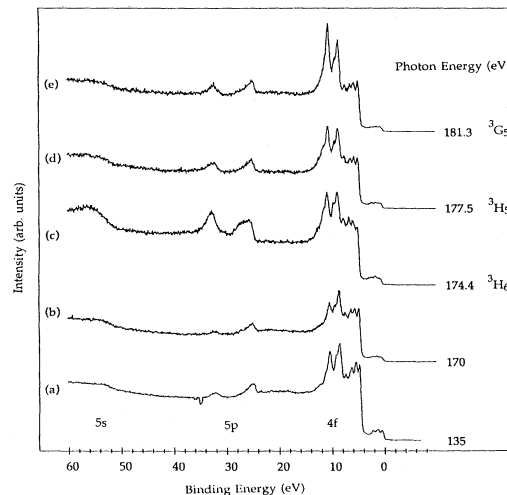


FIG. 2. Electron distribution curves (from 0–60-eV binding energy) measured off and on resonance, at the energies indicated.

between binding energies of 4 and 12 eV is due to trivalent  $4f$  photoemission, and has previously been modeled by Gerken<sup>26</sup> using an intermediate coupling scheme. Divalent Tm emission is also apparent, and is identified by the triplet of peaks from 0- to 4-eV binding energy. This signature for divalent Tm has previously been identified.<sup>27,30,31</sup> Domke *et al.*<sup>27</sup> have grown Tm on a cooled copper surface, and the agreement of the data shown in Fig. 2(a) (off resonant) with the published spectrum is excellent. The divalent  $5s$  and  $5p$  peaks are too weak to be observed.

The other EDC's shown in Fig. 2 are measured using the incident photon energies as labeled in the figure. The changes visible in the peaks will be discussed in the following subsections, with particular emphasis on the  $5p$  and  $4f$  energy levels, for which calculations are also included. As with the absorption spectra calculations, these give the relative energies and intensities of the peaks, allowing the freedom for the spectra as a whole to be moved along the energy axis, giving the best fit to the experimental data. It must be emphasized, however, that the shift in energy must be the same for all spectra.

### C. $5s$ photoemission

As the photon energy is increased, the  $5s$  peak is unchanged through the low-energy side of the absorption spectrum. At 174.4 eV (the  ${}^3H_6$  absorption peak) there is an abrupt change, with the  $5s$  peak apparently increasing in magnitude. It then reduces to its original level. This enhancement at a binding energy of 57 eV and a photon energy of 174.4 eV is due to a  $5p^4 4f^{13}$  final state and not as might have been thought a  $5s^1 4f^{12}$  final state which is at  $\sim 3$  eV lower binding energy. The  $5p^4 4f^{13}$  final state is forbidden in direct photoemission. It has a maximum intensity at the same photon energy as the  $5p^5 4f^{12}$  final state but is at roughly twice the binding energy (Fig. 2).

#### D. 5*p* photoemission

Figures 3(a)–3(e) show the progression of the Tm 5*p* photoemission doublet with incident photon energy. The background has not been subtracted; the spectra are plotted on an absolute intensity scale (with each curve offset for clarity). Corresponding calculations, following absorption to the level shown in Fig. 1(b), of the 5*p* levels, are shown in Figs. 3(f)–3(j); they allow for transitions of the type 4*d*4*f*5*p*.

The photoelectron peaks already show small differences in the relative peak intensities at 170 eV, in comparison to the off-resonant spectrum. When the photon energy reaches the first absorption peak at 174.4 eV, there is an increase in intensity of the photoelectron peaks which is attributed to the interference between the 4*d*4*f*5*p* decay and the direct 5*p* photoemission. This is reflected in the calculated spectrum of Fig. 3(h), which is noticeably stronger than those for lower photon energies [Figs. 3(f) and 3(g)]. The measured spectrum [Fig. 3(c)] also shows a noticeable broadening of the 5*p*<sub>3/2</sub> peak at 174.4-eV photon energy. This behavior is confirmed by the calculation, which indicates an enhancement of the relative strength of the small feature on the low-energy side of the main 5*p*<sub>3/2</sub> peak, between 26 and 28 eV [Fig. 3(b)]. It is clear that the changing shape of the 5*p* peaks at the absorption threshold is the result of the interplay between the magnitude of the Slater integrals, spin-orbit interactions, and Auger matrix elements.

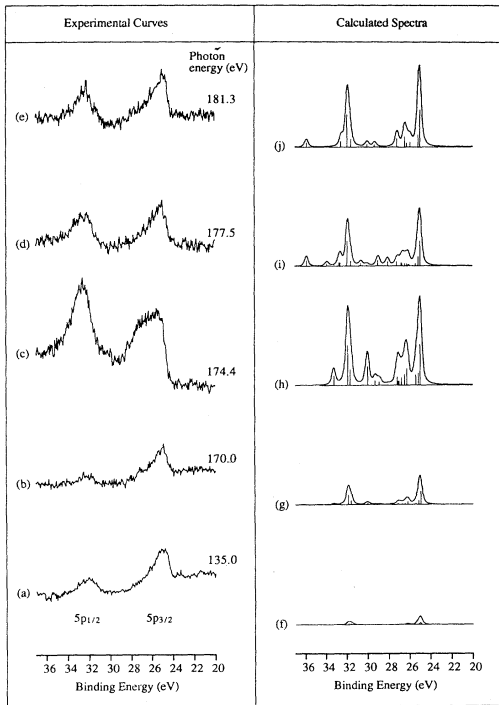


FIG. 3. Tm 5*p* peaks (a)–(e) measured using photons of the indicated energy, with no background subtracted. Calculations at the same points are included (f)–(j) for comparison. The same arbitrary intensity scale has been used for each column of spectra.

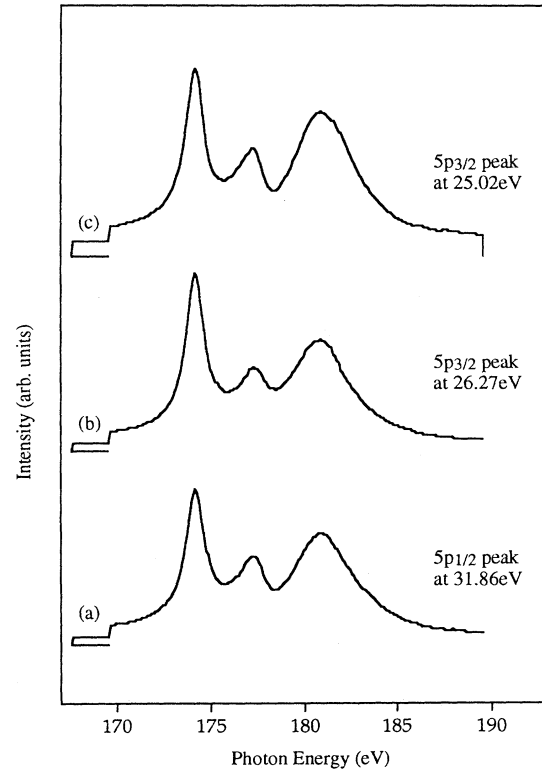


FIG. 4. Constant-initial-state (CIS) calculations for the 5*p* states indicated. The direct photoemission intensity (the non-resonant part) is indicated by the vertical line to the left of each figure.

The photoemission spectra for the higher photon energies [Figs. 3(d) and 3(e)] are similar in shape, though more intense, to the off-resonant spectra [Figs. 3(a) and 3(b)]. Measurement of the area under the peaks indicates a slight increase in intensity between 177.5 and 181.3 eV, as predicted by the model [compare Figs. 3(i) and 3(j)].

Figure 4 shows the calculated constant-initial-state (CIS) spectra of the 5*p* emission. The three curves correspond to the main 5*p*<sub>1/2</sub> and 5*p*<sub>3/2</sub> levels, Figures 4(a) and 4(c), respectively, and the peak on the high-binding-energy side of the 25-eV peak, Fig. 4(b). The curves are all similar in shape to each other and to the absorption spectrum in Fig. 1. The relative strength of the peak at 174.4 eV is greatest for the binding energy of 26.27 eV [Fig. 4(b)], consistent with the appearance of the high-energy shoulder on the 5*p*<sub>3/2</sub> peak in Fig. 3(c).

#### E. 4*f* photoemission

##### 1. Trivalent Tm

Figure 5 shows a direct comparison, on an absolute intensity scale, of the measured [Figs. 5(a)–5(e)] and calculated [Figs. 5(f)–5(j)] trivalent 4*f* spectra at photon energies on and off resonance. It should be noted that no background has been subtracted in the experimental curves, and the resolution in the calculations, given by

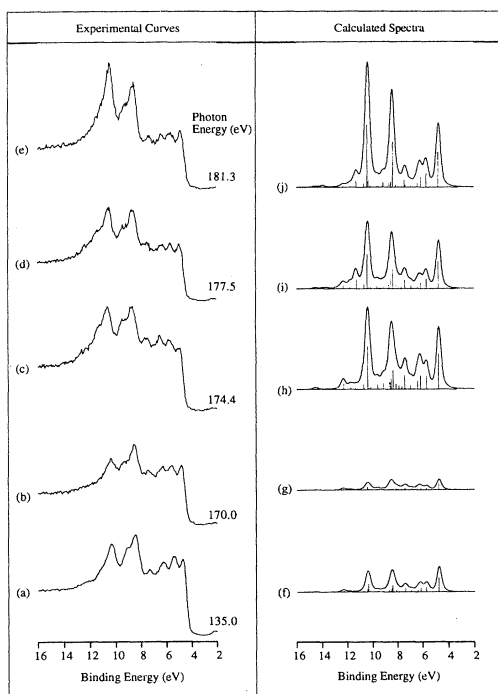


FIG. 5. Tm  $4f$  peaks (a)–(e) measured using photons of the indicated energy, with no background subtracted. Calculations at the same points are included (f)–(j) for comparison. The same arbitrary intensity scale has been used for each column of spectra.

the convolution of Gaussian and Lorentzian functions, is much higher than experimentally observed. This allows a clearer identification of the resonating peaks. The apparent resolution of the experimental curves is reduced by the presence of a surface-shifted component of the trivalent signal (0.7 eV higher in binding energy), which can clearly be seen as shoulders on the high-binding-energy side of the main peaks. This effect is well documented,<sup>32</sup> and these results are consistent with those findings.

The multiplet structure of the trivalent  $4f$  photoemission (shown between 4 and 12 eV in Fig. 2) has previously been calculated by Gerken<sup>26</sup> using an intermediate coupling scheme. The energy positions included a nonphysical scaling factor of 1.1 which was necessary for agreement with the experimental energy positions. The calculations presented here for the  $4f$  energy-level multiplet require no such *a posteriori* scaling factor as the Slater integrals have been reduced to 80–60% of the Hartree-Fock values, to account for intra-atomic correlation effects. The multiplet calculation leads to a discrete energy spectrum [Fig. 5(f)], which is then broadened using Gaussian and Lorentzian functions.<sup>29</sup> The agreement with the experimentally measured spectrum [Fig. 5(a)] is good. The fit could be improved by including the surface-shifted trivalent emission, by moving the bulk trivalent spectrum in energy and reducing the intensity, consistent with the lower number of trivalent surface

atoms.

At the energies of the three absorption peaks; 174.4 ( ${}^3H_6$ ), 177.5 ( ${}^3H_5$ ), and 181.3 eV ( ${}^3G_5$ ), mainly three features show resonant enhancement. These are at binding energies of 10.3, 8.5, and 4.5 eV. The calculations show that at all three absorption peaks the enhancement is due to processes of the form  $4d4f4f$ . The resonantly emitted  $4f$  electron will have the same energy as the directly emitted  $4f$  photoelectron, causing an enhancement of the observed peak intensity.

Calculated CIS spectra for the three main  $4f$  peaks are shown in Fig. 6. We note that the curve at 4.5 eV has a lower intensity than the 10.3- and 8.5-eV peaks. This is consistent with the observation that the 10.3- and 8.5-eV peaks are preferentially enhanced throughout the absorption energy range. The calculations also confirm the observation that, whereas the 10.3-eV peak and the 8.5-eV one are of similar intensity at photon energies of 174.4 and 177.5 eV, the 10.3-eV emission is significantly larger for photons of energy 181.3 eV. It is interesting to note that the spectra in Fig. 6 show normal Fano profiles<sup>33</sup> with a dip before the main peak, in contrast to the CIS curves of the  $5p$  levels in Fig. 4. This explains the relative enhancement of the  $4d5p4f$  process compared to the  $4d4f4f$  one at a photon energy of 174.4 eV, in Fig. 2(c).

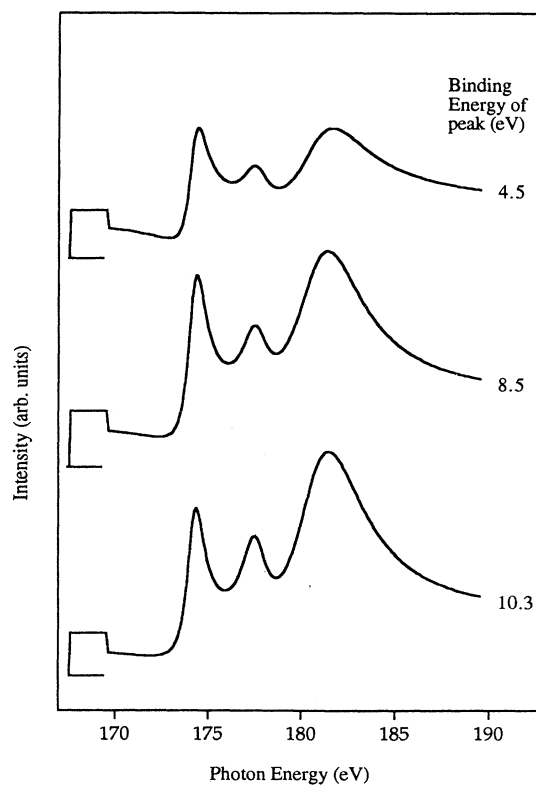


FIG. 6. Constant-initial-state (CIS) calculations for the  $4f$  states indicated. The direct photoemission intensity (the non-resonant part) is indicated by the vertical line to the left of each figure.

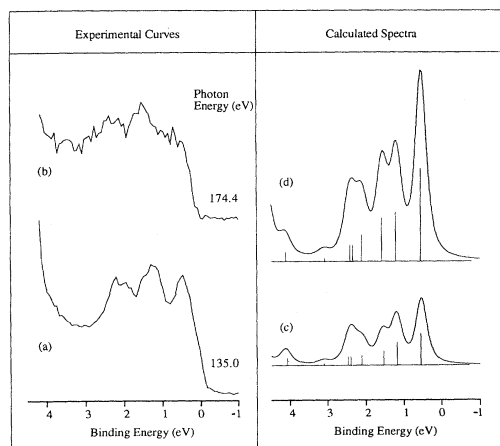


FIG. 7. Divalent Tm 4f peaks (a) and (b) measured using photons of the indicated energy, with no background subtracted. Calculations at the same points are included (c) and (d) for comparison.

## 2. Divalent Tm

The photoemission features from the 4f levels of divalent Tm occur in the binding-energy range 0–4 eV and are clearly visible in the 135-eV spectrum of Fig. 7(a). The calculated absorption spectrum for divalent Tm indicates a single peak at an energy close to the  ${}^3H_6$  trivalent absorption peak. Therefore, the resonance should be observable in the 174.4-eV spectrum of Fig. 7(b). The calculated spectra indicate the resonance of the triplet of peaks to be weak, with an increase of only three times the original photoemission intensity. There is some evidence of an enhancement in Fig. 7(b), with the central peak of the three becoming more prominent, which may be due to the overlap of the two small central peaks. The increase is again predicted to be due to  $4d4f4f$  processes, where the 4f level involved is from the divalent  $4f^{13}$  Tm ground state. There is no evidence of any resonance at higher photon energies, with the 0–4-eV region being very flat.

## V. CONCLUSIONS

The absorption spectrum for thick layers of Tm deposited at 150 K on an Ag(001) surface shows three strong absorption peaks; the  ${}^3H_6$  at 174.4 eV, the  ${}^3H_5$  at 177.5 eV, and the  ${}^3G_5$  at 181.3 eV.

The decay of the 4d hole following resonant absorption

into the 4f energy level has been monitored in Tm by photoelectron spectroscopy, and modeled by calculations predicting emission intensities. The absorption peak resulting in a  ${}^3H_6$  final state shows enhancement of predominantly the 5s and 5p energy levels, and some increase in the divalent and trivalent 4f states. This can be explained by Fano antiresonance behavior of the  $4d4f5p$  emission compared to the normal Fano profile of the  $4d4f4f$  emission. The weak peak ( ${}^3H_5$ ) leads to a small relative increase in the emission through the trivalent 4f channel at 10.3 eV. The third absorption peak ( ${}^3G_5$ ) shows strong enhancement at binding energies of 10.3 and 8.5 eV, in the trivalent 4f emission, relative to other peaks.

There is evidence of a small enhancement of the divalent signal at a photon energy of 174.4 eV, which is predicted to be close to the divalent absorption peak maximum. This is consistent with a  $4d4f4f$  process involving divalent Tm.

In all cases, the observed enhancements are predicted by calculations which allow for direct recombination into the 4d hole (i.e., processes of the type  $4d4fX$ , where  $X=5s, 5p$ , or  $4f$ ). It can therefore be concluded that in Tm the decay of the 4d hole following absorption is solely by direct recombination, resulting in enhancement of the directly emitted photopeaks.

We have demonstrated that we obtain good agreement between experimental results and theoretical calculations for both the  $4d4f4f$  and  $4d4f5p$  resonant decays, using only scaling factors for the Slater integrals and Auger matrix elements. This opens the way for (spin polarized) photoemission on magnetic rare earths, using circularly or linearly polarized x rays, since, given that the isotropic spectrum is determined, the magnetic dichroism and the spin spectrum in localized materials depend only on the angular momentum coupling.<sup>34</sup> The latter is determined by the coupling regime, e.g., *LS* or *jj* coupling, or more generally, as in this case, intermediate coupling. As has recently been shown for nickel in Ref. 35, measurement of the magnetic dichroism in resonant photoemission provides a promising way to obtain ground-state magnetic moments of magnetic materials.

## ACKNOWLEDGMENTS

We wish to thank J. S. G. Taylor and S. C. Thornton for their expert technical assistance. This work has been supported by the Science and Engineering Research Council: Grant No. GR/F 17667. Financial support by the CNRS (PICS No. 51) is also acknowledged.

<sup>1</sup>B. Johansson, Phys. Rev. B **19**, 6615 (1979).

<sup>2</sup>G. R. Stewart, Rev. Mod. Phys. **56**, 755 (1984).

<sup>3</sup>B. T. Thole, G. van der Laan, J. C. Fuggle, G. A. Sawatzky, R. C. Karnatak, and J.-M. Esteve, Phys. Rev. B **32**, 5107 (1985).

<sup>4</sup>L. I. Johansson, J. W. Allen, and I. Lindau, Phys. Lett. **86A**, 442 (1981).

<sup>5</sup>W. Lentz, F. Lutz, J. Barth, G. Kalkoffen, and C. Kunz, Phys. Rev. Lett. **41**, 1185 (1978).

<sup>6</sup>A. Zangwill, in *A Condensed Matter View of Giant Resonance Phenomena in Giant Resonances in Atoms, Molecules, and*

*Solids*, edited by R. Karnatak, J.-M. Esteve, and J. P. Connerade (Plenum, New York, 1987), p. 319.

<sup>7</sup>J. L. Dehmer, A. F. Starace, U. Fano, J. Sugar, and J. W. Cooper, Phys. Rev. Lett. **26**, 1521 (1971).

<sup>8</sup>F. Gerken, J. Barth, and C. Kunz, in *X-ray and Atomic Inner-Shell Physics*, edited by B. Crasemann, AIP Conf. Proc. No. 94 (AIP, New York, 1982).

<sup>9</sup>A. F. Starace, Phys. Rev. B **5**, 1773 (1972).

<sup>10</sup>J. Sugar, Phys. Rev. B **5**, 1785 (1972).

<sup>11</sup>J. L. Dehmer and A. F. Starace, Phys. Rev. B **5**, 1792 (1972).

- <sup>12</sup>P. A. Dowben, D. LaGraffe, D. Li, L. Döttl, C. Hwang, Y. Ufuktepe, and M. Onellion, *J. Phys. Condens. Matter* **2**, 8801 (1990).
- <sup>13</sup>J. A. D. Matthew, G. Strasser, and F. P. Netzer, *J. Phys. C* **15**, L1019 (1982).
- <sup>14</sup>G. Rossi, J. J. Yeh, I. Lindau, and J. Nogami, *Surf. Sci.* **152/153**, 743 (1985).
- <sup>15</sup>F. P. Netzer, E. Bertel, and J. A. D. Matthew, *J. Phys. C* **14**, 1891 (1981).
- <sup>16</sup>H. Ogawasara, A. Kotani, B. T. Thole, K. Ichikawa, O. Aita, and M. Kamada, *Solid State Commun.* **81**, 645 (1992).
- <sup>17</sup>G. Rossi, J. J. Yeh, I. Lindau, and J. Nogami, *Phys. Rev. B* **29**, 5989 (1984).
- <sup>18</sup>F. U. Hillebrecht, *Phys. Rev. B* **41**, 5583 (1990).
- <sup>19</sup>N. Mårtensson, *Z. Phys. B* **61**, 457 (1985).
- <sup>20</sup>G. van der Laan, M. Surman, M. A. Hoyland, C. F. J. Flipse, B. T. Thole, Y. Seino, H. Ogasawara, and A. Kotani, *Phys. Rev. B* **46**, 9336 (1992).
- <sup>21</sup>G. van der Laan, B. T. Thole, H. Ogasawara, Y. Seino, and A. Kotani, *Phys. Rev. B* **46**, 7221 (1992).
- <sup>22</sup>O.-P. Sairanen, S. Aksela, and A. Kivimäki, *J. Phys. Condens. Matter* **3**, 8707 (1991).
- <sup>23</sup>O.-P. Sairanen and S. Aksela, *J. Phys. Condens. Matter* **4**, 3337 (1992).
- <sup>24</sup>L. I. Johansson, J. W. Allen, and I. Lindau, *Phys. Lett.* **86A**, 442 (1981).
- <sup>25</sup>S.-J. Oh, J. W. Allen, and I. Lindau, *Phys. Rev. B* **30**, 1937 (1984).
- <sup>26</sup>F. Gerken, *J. Phys. F* **13**, 703 (1983).
- <sup>27</sup>M. Domke, M. Laubschat, M. Prietsch, T. Mandel, G. Kaindl, and W. D. Schneider, *Phys. Rev. Lett.* **56**, 1287 (1986).
- <sup>28</sup>R. D. Cowan, *The Theory of Atomic Structure and Spectra* (University of California Press, Berkeley, 1981).
- <sup>29</sup>P. A. Cox, *J. Electron Spectrosc. Relat. Phenom.* **22**, 77 (1981).
- <sup>30</sup>M. Prietsch, M. Domke, C. Laubschat, and G. Kaindl, *Phys. Rev. B* **38**, 10655 (1988).
- <sup>31</sup>M. Prietsch, M. Domke, C. Laubschat, and G. Kaindl, *Phys. Rev. Lett.* **60**, 436 (1988).
- <sup>32</sup>F. Gerken, A. S. Flodström, J. Barth, L. I. Johansson, and C. Kunz, *Phys. Scr.* **32**, 43 (1985).
- <sup>33</sup>U. Fano, *Phys. Rev.* **124**, 1866 (1961).
- <sup>34</sup>B. T. Thole and G. van der Laan, *Phys. Rev. B* **44**, 124 (1992); G. van der Laan and B. T. Thole, *ibid.* **48**, 210 (1993).
- <sup>35</sup>B. T. Thole, H. A. Dürr, and G. van der Laan, *Phys. Rev. Lett.* **74**, 2371 (1995).